



# Finite Element Model Prediction of Charge Weld Behaviour in AA6082 and AA6063 Extruded Profiles

Marco Negrozio, Riccardo Pelaccia, Lorenzo Donati, Barbara Reggiani, Tommaso Pinter, and Luca Tomesani

Submitted: 16 November 2020 / Revised: 18 February 2021 / Accepted: 19 March 2021 / Published online: 16 April 2021

**Charge welds are unavoidable defects of the continuous extrusion process whose extension needs to be accurately predicted in order to avoid profile mechanical failures or to minimize unrequired scrap of material. The aim of this work was then to evaluate the accuracy of the charge welds FEM predictions and their applicability in the industrial field. Two different industrial cases involving A6082 and AA6063 aluminium alloys were analysed. The data of charge welds behaviours were experimentally collected, discussed and then innovatively compared to the predicted outcomes of FEM simulations performed using QForm Extrusion® software and of theoretical formulas reported in the literature. As main results, a very good numerical-experimental matching was found, with a peak discrepancy of 122 mm in terms of charge weld extent, while theoretical formulas returned a significant underestimation.**

**Keywords** aluminium alloys, charge welds, extrusion, FEM, microstructure, 6063, 6082

## 1. Introduction

The extrusion of Al–Mg–Si aluminium alloys is a widely used manufacturing process that represents a competitive solution to produce profiles with complex geometries and constant cross sections. These profiles are used in sectors such as civil, industrial and automotive due to their good extrudability and their high mechanical and aesthetical properties, which make these alloys particularly suitable for these fields (Ref 1-3). For structural applications, mechanical properties must be consistent throughout the extent of the profile, so that structural defects cannot be tolerated.

Charge welds (also called front-end defect), which occur at the beginning of each extruded profile during the extrusion of multiple billets, compromise the mechanical properties and lead to the material scrap (Ref 4, 5). In Fig. 1(a), an example of this behaviour is shown: at the start of each press cycle, when the extrusion begins, the new (red) billet material flows inside the die interpenetrating the old (blue) one left from the extrusion of the previous billet, thus generating a welding zone that extends to a certain profile length till the complete old-new billet replacement.

The new-old billet welding surface is contaminated by impurities (oxides, dust or lubricant) accumulated during the loading of the new billet. These contaminations cause a loss of

mechanical properties, and for this reason, scraping of material is needed. This scrap starts from the stop mark, which is a visible mark on the profile surface generated by the adhesion of the material on the bearing zone during the billet replacement (Fig. 1b) and ends up at the point where the profile cross section contains only the new billet material ( $d$  in Fig. 1a). On the transverse section of the profile, the charge weld appears as a closed contour containing the material of the new incoming billet that gradually enlarges approaching the profile surface until the complete replacement (Fig.1c).

The methodologies used to experimentally analyse the evolution of the charge welds require time-consuming activities such as cutting, grinding and etching of the extruded profile, and the results of these analyses can be referred only to the specific profile and die-set geometries. In addition, the experimental analyses can be carried out only after the production of the involved extrusion die and tool set, leading to additional costs that could be avoided by optimizing the geometries at the design stage. For these reasons, the prediction of the charge weld position and extent through numerical methods as the finite element (FE) one became of great interest for the extruders and die makers, and consequently, the accuracy of these methods requires an adequate investigation and validation.

Among the different commercial FE codes available to simulate the extrusion process, QForm® and the dedicated auxiliary module QForm extrusion® are attracting interest by researchers, extruders and die makers given their capabilities to solve problems encountered in extruding complex shapes, designing new tools, selecting process parameters and identifying possible defects (Ref 6-10). If the QForm code is based on a Lagrange approach with the mesh that flows with the material inside the die, thus offering a comprehensive knowledge of the die filling stage but requiring a lot of remeshing, QForm Extrusion is based on a combined Lagrange–Euler approach resulting to be more suitable for the investigation of complex dies and profiles (Ref 6).

Concerning the charge welds prediction, in recent years many studies have been performed in order to investigate the defect behaviour and the accuracy of its prediction methods. Den Bakker AJ et al. (Ref 11) studied the effect of the presence

Marco Negrozio, Lorenzo Donati, and Luca Tomesani, DIN Department of Industrial Engineering, University of Bologna, Viale Risorgimento 2, 40136 Bologna, Italy; Riccardo Pelaccia and Barbara Reggiani, DISMI Department of Sciences and Methods for Engineering, University of Modena and Reggio Emilia, Via Amendola 2, 42122 Reggio Emilia, Italy; Tommaso Pinter, Almax Mori, Via Matteotti 13, 38065 Mori, Italy. Contact e-mail: marco.negozio2@unibo.it.

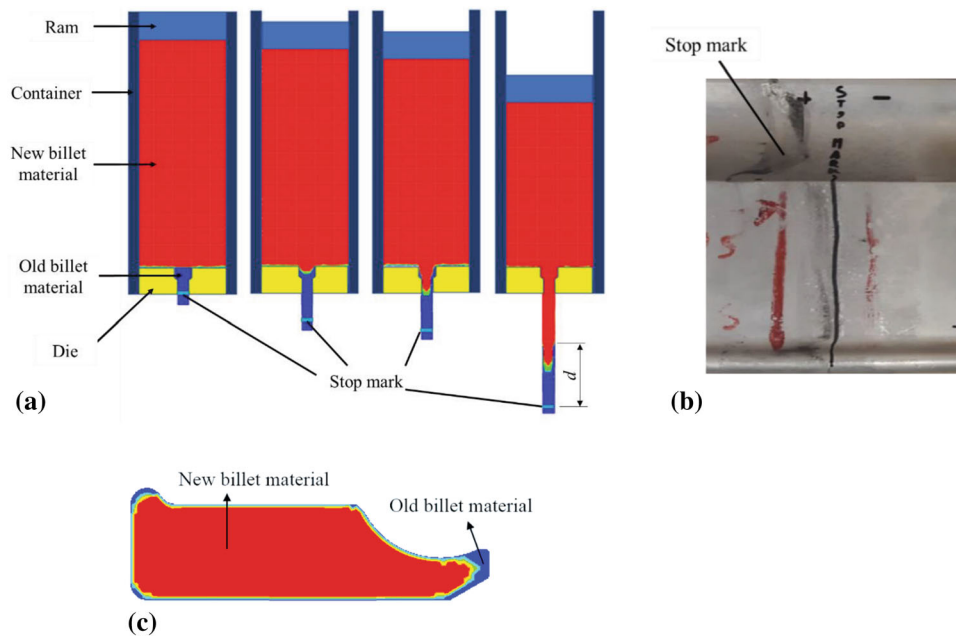


**Fig. 1** (a) charge weld generation during the extrusion of multiple billets (“ $d$ ” is the extent of the charge weld), (b) evidence of the stop mark in the investigated profile, (c) charge weld in the cross section of an extruded profile

of a charge welds transition zone on the failure mode and local effective mechanical properties of the extrudate, Nanninga et al. (Ref 12) evaluated the fatigue properties of specimens where charge welds occur while Valberg H et al. (Ref 4) investigated the preventive measures that can be made by the extruder companies to avoid the formation of such defect. About FEM simulations, several authors assessed the defect predictability for extruded profiles of industrial complexity using an Arbitrary Lagrangian–Eulerian approach with HyperXtrude® software (Ref 13–19) others using the FE code Deform2D on an axisymmetric case (Ref 20, 21). Although these several studies on the charge weld prediction, further investigations are still needed in order to validate the accuracy of FEM codes against industrial profiles of variable geometries, material properties and process parameters. In particular, to the best of the author’s knowledge, no previous studies investigated the charge welds using the FEM code QForm Extrusion.

For a faster charge welds extent computation, two theoretical formulae have been proposed in the past in literature that are reported in Eq 1 and 2 (Ref 22, 23) in which  $d$  is the charge weld extent (Fig. 1a):

$$d = \frac{(V1 + V2)}{Ae \times n} \quad (\text{Eq 1})$$

$$d = 1.5 * \frac{(V1 + V2)}{Ae \times n} \quad (\text{Eq 2})$$

In Eq 1,  $d$  has been related to the volume of material presents in the die ports  $V1$  and in the welding chamber  $V2$ , to the exit profile section area  $Ae$  and to the number of openings in the die  $n$ .

In Eq 2, a corrective factor 1.5 was proposed by Jowett et Al. (Ref 23) to provide a better match with the experimental data. They introduced the corrective factor for two reasons: on the one hand, the metal flowing in the profile is not the entire port volume due to the presence of dead metal zones. On the

other hand, the flow of the material is always faster in the centre of the ports as consequence of the steel–aluminium friction. These two effects extend the defect respect to the prediction provided by Eq 1, and Jowett et Al. (Ref 23) proposed the 1.5 coefficient used in Eq 2.

In this context, the aim of this work was to investigate the predictability of charge welds behaviour with the QForm Extrusion code for two industrial profiles made of AA6082 and AA6063 alloys by comparing the numerical results with experimental data. In addition, outcomes were also compared to the prediction of the two theoretical formulas reported in Eq 1 and 2.

## 2. Experimental Procedure

The geometries of the two investigated extruded profiles and dies are shown in Fig. 2(a), (b): both profiles (in the following labelled as A and B) are solid, and they were produced by Indinvest LT plant of Latina (Italy) on an industrial 35 MN press. Profile A has a cross-sectional area of 598.93 mm<sup>2</sup> and an extrusion ratio of 44 while profile B 2761.35 mm<sup>2</sup> and 20, respectively. As can be seen, profile A is marked by a central thick section with a thin, jagged appendix, thus suggesting a quite inhomogeneous material flow and, consequently, a challenging billets-replacement dynamic. Profile B, on the contrary, has a more uniform thickness and is more massive.

Profile A is made by AA6063 and was manufactured using a flat two-holes die (Fig. 2c) while the profile B is made by AA6082 and has been extruded using a flat die with a single die opening (Fig. 2d). Fifty billets were extruded for each production batch, and the investigated profiles sections were extracted in the transitions between the 6th and the 7th billets for each batch in order to be sure to select a steady-state process condition.

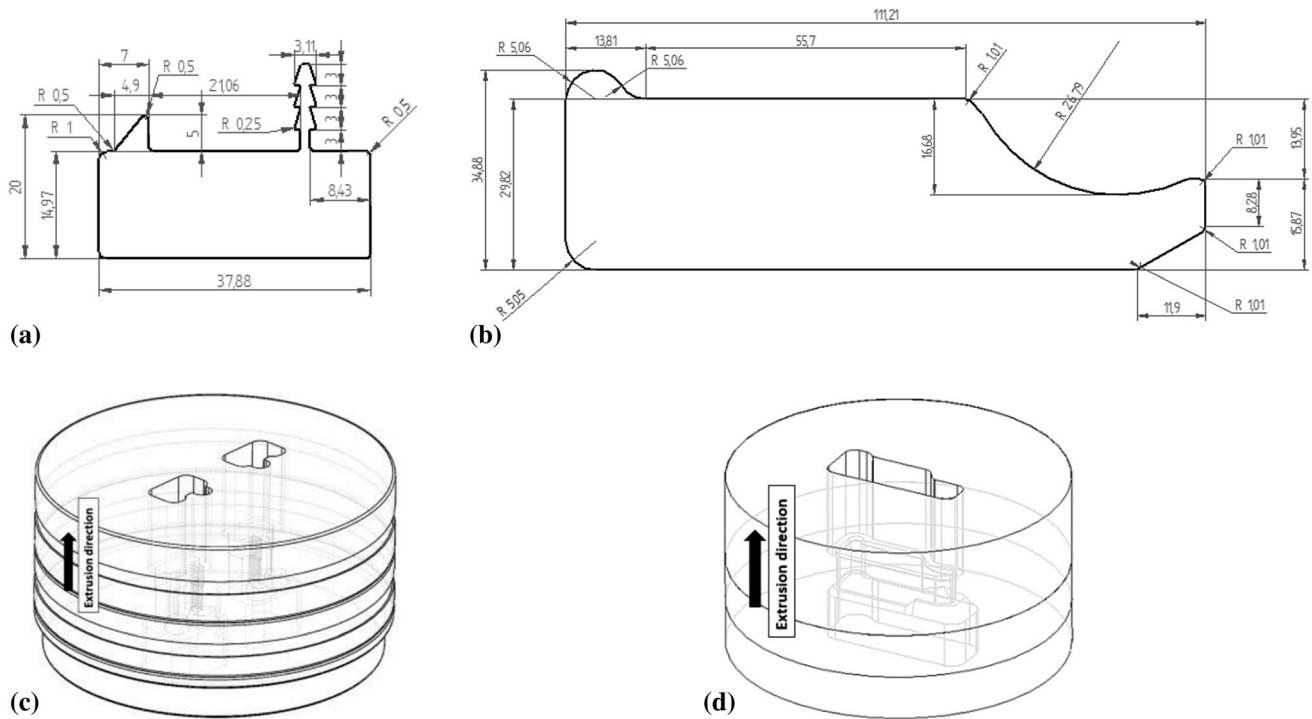


Fig. 2 Geometries of the profiles and of the dies under investigation: a, c profile A, b, d profile B

Table 1 Process parameters and geometry tolerances

| Process parameters and geometry tolerances | Profile A | Profile B |
|--|-----------|-----------|
| Aluminium alloy                            | AA6063    | AA6082    |
| Extrusion ratio                            | 44        | 20        |
| Ram speed, mm/s                            | 6.44      | 7.64      |
| Container temperature, °C                  | 430       | 440       |
| Billet temperature, °C                     | 530       | 530       |
| Die temperature, °C                        | 450       | 450       |
| Ram acceleration time, s                   | 5         | 5         |
| Billet length, mm                          | 670       | 990       |
| Billet diameter, mm                        | 254       | 254       |
| Container diameter, mm                     | 264       | 264       |
| Billet Rest length, mm                     | 15        | 15        |

In Table 1, the extrusion process and the tools geometry parameters are reported. As can be seen, the initial temperature of the die, billet and container as well as the ram acceleration time and speed, the billet rest length, the container and billet diameters were similar for both profiles. The main differences were detected in the extrusion ratio (44 for profile A and 20 for profile B) and in terms of billet length (990 mm for profile A and 670 mm for profile B).

After the cooling down of the profile and before the heat treatment, a length of 2100 mm was collected for both profiles after the stop mark for the charge welds evolution assessment; the length was selected accounting for the standard industrially scrapped portions of around 2000 mm (Ref 14). The profiles were initially cut into samples of 100 mm; then, for the extent of the profiles in which the defect was expected to increase rapidly, samples were further sectioned for an in-depth investigation of the charge weld evolution. All the samples

were then grinded with abrasive papers and subsequently etched in sodium hydroxide solution 30% in H<sub>2</sub>O (300g of NaOH for 1 l of H<sub>2</sub>O heated to 60 °C, etching time in the range of 45-90 sec) on the same side with respect to the extrusion direction. This etching was made with the aim to reveal the charge welds defect on the cross section of each samples making, as proved by Fig. 3, the macrostructure of the defects immediately visible to unaided eyes.

In order to assess and quantify the defect pattern, each section was acquired through digital photography and the charge welds identified by colouring and measuring the area of the contour enclosing the new billet material. In the performed analysis, it was assumed that the extinction of the defect occurred at the 99% of the replacement (while in industry such value is nearer to a 95%) accounting for the difficulties in evaluating the material behaviour when the new billet approaches the profile surface.

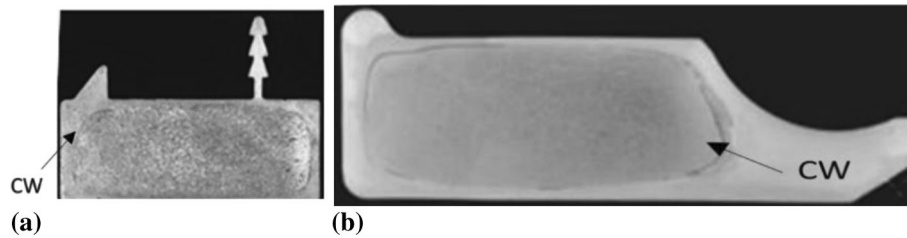


Fig. 3 Cross section of the profiles after etching: (a) profile A; (b) profile B

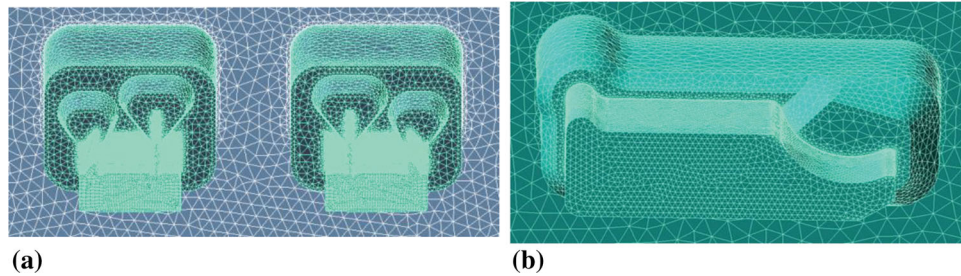


Fig. 4 FE models of the investigated profiles: (a) profile A, (b) profile B

### 3. Numerical Procedure

The two investigated case studies have been simulated by means of the FE code QForm Extrusion, which is an ALE (Arbitrarily Lagrangian–Eulerian) tool of QForm code optimized for the simulation of the extrusion process (Ref 24, 25). For the preparation of the tools/workpiece 3D geometries, a QForm internal program, QShape, was used to generate the volumetric meshes of tools and of the billet materials in the already extruded shape (Fig. 4). Mesh parameters are reported in detail in Table 2.

As constitutive model for the extruded materials, the following Hensel–Spittel law was selected due to its ability in accurately representing the relationship between the main parameters affecting the flow stress, i.e. strain, strain rate and temperature (Ref 26):

$$\bar{\sigma} = A \cdot e^{m_1 T} \cdot \bar{\epsilon}^{-m_2} \cdot \dot{\bar{\epsilon}}^{-m_3} \cdot e^{\frac{m_4}{T}} \cdot (1 + \bar{\epsilon})^{m_5 T} \cdot e^{m_7 \bar{\epsilon}} \cdot \dot{\bar{\epsilon}}^{m_8 T} \cdot T^{m_9} \quad (\text{Eq 3})$$

where  $\bar{\sigma}$  is the flow stress,  $\bar{\epsilon}$  the strain,  $\dot{\bar{\epsilon}}$  the strain rate,  $T$  the temperature (K) and  $A, m_1$ – $m_9$  material parameters to be regressed over experimental trials.

Different parameters of the H-S law can be found for the same nominal alloy (chemical composition within the alloy ranges) by checking literature, codes databases or by performing experimental trials. For this reason, a sensitivity study of the flow stress parameters on charge weld evolution was included in this study. Two different combinations of material parameters were tested (Table 3): L1 values were set according to the regression performed by El Mehtedi et al. (Ref 27), L3 values to a study performed by Selvaggio A. et al. (Ref 28), and L2 and L4 values were set according to the QForm database.

The other thermal and physical properties used for the numerical simulations of the two investigated alloys were set to the default values contained in the QForm database.

### 4. Results and Discussion

#### 4.1 Experimental Results

In Fig. 5 and 6, the experimental evolution of charge welds for A and B profiles is shown following the distance ‘ $d$ ’ from the stop mark. In Fig. 5(a), it can be noticed that the charge in profile A already invested a significant portion of the section at a distance of 147 mm from the stop mark proving, as expected, a fast flowing of the material in the massive part of the profile. In addition, Fig. 5(a) and (b) shows the presence not only of the charge weld (CW) but also of the billet skin (BS), a defect generated by the progressive accumulation of a thin contaminated billet layer in the rear end due to the progressive advancement of the ram (Ref 15). Figures clearly show the dynamic interaction of the two phenomena with the BS defect that is gradually moved aside till its complete disappearance between 161 mm and 198 mm from the stop mark. After that point, the charge weld rapidly increases approaching an 86% of old-new billet replacement at +297 mm from the stop mark. At +297 mm, the new billet material within the charge weld starts to flow into the jagged thin and in the triangular details of the profile, then continuing more slowly until the defect extinction at +880 mm.

In profile B (Fig. 6), the BS defect starts to flatten out and moving toward the bottom part of the profile at +68 mm (Fig. 6a), thus suggesting the upcoming of the charge weld defect that reaches the 90% of replacement at +190 mm (Fig. 6d) and the 99%, and consequently its extinction, at +400 mm (Fig. 6h).

In both profiles, the start of the defect contamination occurs in the centre of the profile, due to the faster and unconstrained flowing of the material, then enlarging up to the complete filling of the sections at the profile surfaces. However, as expected, profile A shows a longer evolution of the charge weld according to the greater extrusion ratio with respect to profile B.

**Table 2 Mesh parameters: number of 4-nodes tetrahedral elements used**

| Object              | Profile A |         |         | Profile B |         |        |
|---------------------|-----------|---------|---------|-----------|---------|--------|
|                     | Workpiece | Die set | Total   | Workpiece | Die set | Total  |
| Nodes on surface    | 52695     | 55772   | 108467  | 17215     | 13493   | 30708  |
| Internal nodes      | 157606    | 183434  | 341040  | 52901     | 41899   | 94800  |
| Total nodes         | 210301    | 239206  | 449507  | 70116     | 55392   | 125508 |
| Surface elements    | 105386    | 111548  | 216934  | 34426     | 26986   | 61412  |
| Volumetric elements | 1123768   | 1296022 | 2419790 | 373987    | 297779  | 671766 |

**Table 3 Hensel–Spittel parameters**

| Hensel–Spittel parameters | Profile A                    |                              | Profile B                    |                             |
|---------------------------|------------------------------|------------------------------|------------------------------|-----------------------------|
|                           | L1                           | L2                           | L3                           | L4                          |
| A                         | 1014,7 [MPa]                 | 265 [MPa]                    | 560000 [MPa]                 | 270 [MPa]                   |
| m1                        | −0.00438 [K <sup>−1</sup> ]  | −0.00458 [°C <sup>−1</sup> ] | −0.002117 [K <sup>−1</sup> ] | −0.0045 [°C <sup>−1</sup> ] |
| m2                        | 0.2425                       | −0.12712                     | 0.1059                       | −0.127                      |
| m3                        | −0.0965                      | 0.12                         | 0.098                        | 0.13                        |
| m4                        | −0.000438                    | −0.0161                      | 0.0009266 [K <sup>−1</sup> ] | −0.016                      |
| m5                        | −0.000766 [K <sup>−1</sup> ] | 0.00026 [°C <sup>−1</sup> ]  | −0.00065                     | 0.00026 [°C <sup>−1</sup> ] |
| m7                        | 0.02939                      | 0                            | 0.02343                      | 0                           |
| m8                        | 0.000291 [K <sup>−1</sup> ]  | 0                            | 0.00006471[K <sup>−1</sup> ] | 0                           |
| m9                        | 0                            | 0                            | −1.208                       | 0                           |

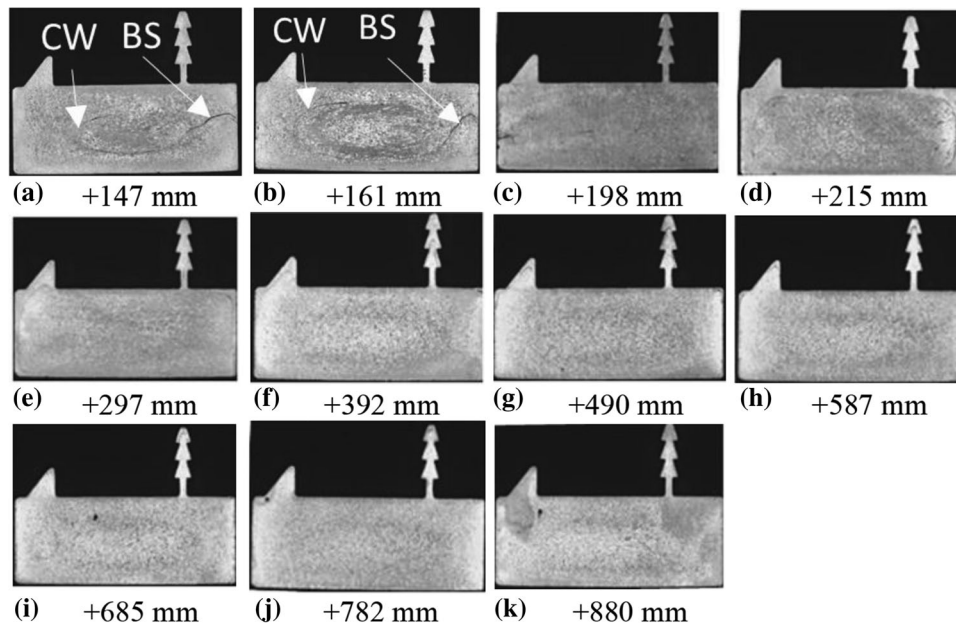


**Fig. 5** Charge weld evolution in profile A

In order to quantitatively assess the charge welds trend, the percentage area containing the new billet material has been computed by means of an image analysis tool of a CAD software on high-resolution pictures of each etched section of the two profiles and reported over the stop mark distance (Fig. 7 and 8). In both profiles, the trend is similar: after the onset of

the defect, a fast material replacement is visible up to the 70–80%; then the evolution curves flatten towards an almost asymptotic behaviour. The extent of the evolution is deeply related to the process extrusion ratio and to the die geometry complexity. The trend found by experimental analyses is in accordance with studies already published in the literature (Ref 14, 16).

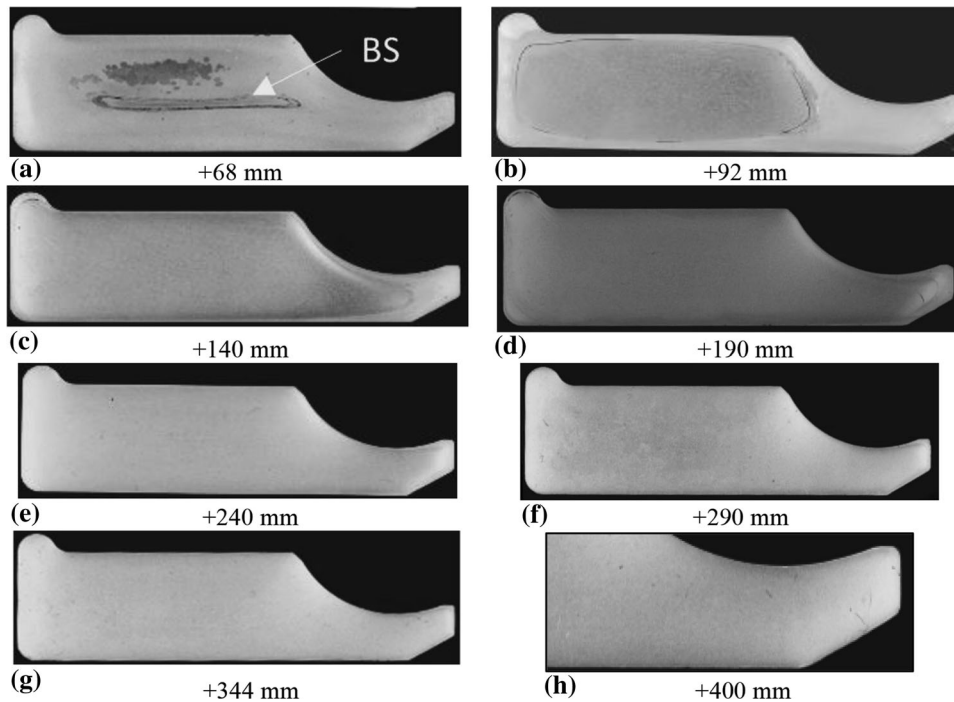


**Fig. 6** Charge weld evolution in profile *B*

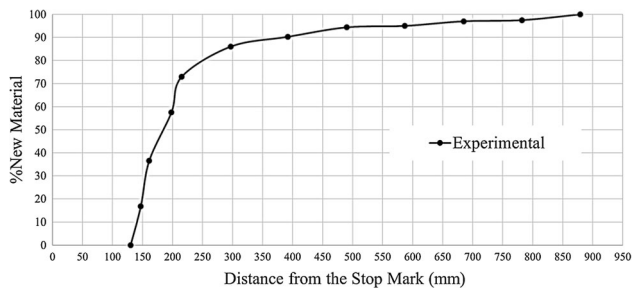


**Fig. 7** Experimental charge weld evolution—Profile *A*

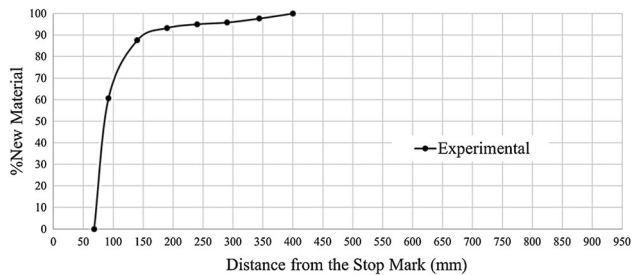


**Fig. 8** Experimental charge weld evolution—Profile *B*

#### 4.2 Numerical and Theoretical Results

The charge welds extension (distance of the extinction point from the stop mark) as predicted by the two theoretical formulae, Eq. 1 and 2 previously reported, are detailed in Table 4.

As can be seen, for profile *A* the end of the charge weld defect is estimated at +240 mm by Eq. 1 and at +361 mm by Eq. 2 while, for profile *B*, at +133 and +199, respectively. In Fig. 9, the discrepancy between the theoretical and experimen-

**Table 4** Theoretical method results

|                 | Extents (distance from stop mark) | Profile <i>A</i> | Profile <i>B</i> |
|-----------------|-----------------------------------|------------------|------------------|
| Theoretical (1) | Charge weld end, mm               | +240             | +133             |
| Theoretical (2) | Charge weld end, mm               | +361             | +199             |

tal results is highlighted with an evident underestimation of the defect extent equal to 72% with Eq. 1 and 59% with Eq. 2 for profile *A*, 67% with Eq. 1 and 50% with Eq. 2 for profile *B*.

In Fig. 10 and 11, the outcomes of the numerical simulations with the two different constitutive equations are compared to the experimental charge welds evolutions. As can be observed, for both profiles, the numerical evolutions L1 and L2 for profile *A*, L3 and L4 for profile *B*, are perfectly stackable. This supports, at least from a numerical point of view, what reported in the literature regarding the charge weld dependency on the die-set and profile geometries and the negligible influence of other process-related variables such as the material flow stress definition, and the billet-die temperatures (Ref 23, 29-31).

Concerning profile *A*, the onset and the extinction of the charge weld were experimentally determined at +130 mm and +880 mm, while numerically predicted at +125 mm (−3,8%) and +801 mm (−9%), respectively, showing an underestimation of 5 mm for the onset and 79 mm of the defect extent. The data of Fig. 9 clearly show that there is an almost perfect overlapping of simulated data over experimental ones, except for the last 5% of contamination transition (95% to 100%) since the numerical trend, after reaching the 95% of new-old billet replacement, abruptly increases up to the 100%.

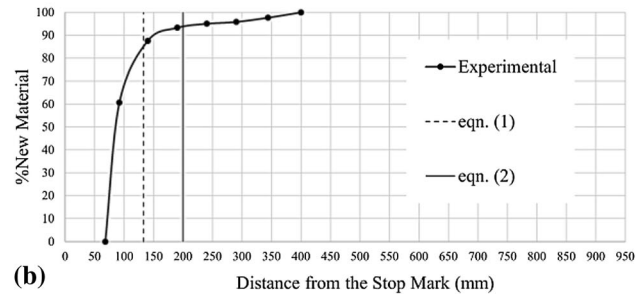
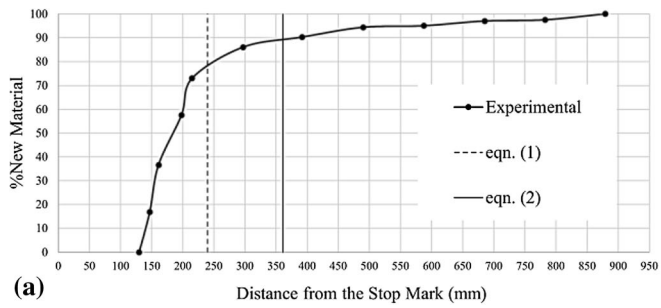


**Fig. 9** Theoretical and experimental charge welds on both profiles

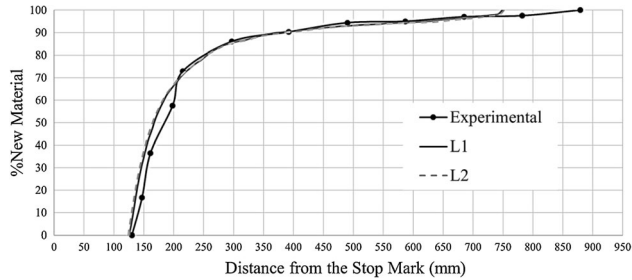


**Fig. 10** Numerical and experimental results of the charge weld evolution – Profile A

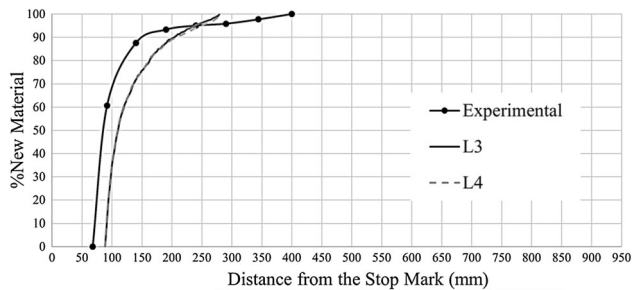


**Fig. 11** Numerical and experimental results of the charge weld evolution – Profile B

For profile B, the experimental onset and extinction points of the charge weld were found at +68 mm and +400 mm, while they were numerically predicted at +85 mm (+25%) and +278 mm (−30%), respectively, showing a slightly overestimation of 27 mm for onset and an underestimation of 122 mm for the defect extent. If the values in % seem critical, it has to be noted that this is a consequence also of the quite fast transition of the B profile (350 mm versus 750 of profile A and versus a value of 2000 mm scrap assessment usually adopted in industrial standards). Indeed, the onset overestimation is limited to 17 mm only: this value is quite below the specimen length resolution usually adopted in industry (200 mm) and also quite below the value initially adopted in this study (100 mm). Concerning the extinction value, even in this case, the numerical curve well approximates the defect behaviour at around the 95% of contamination and, after that point, it rapidly increases up to the 100%.

The behaviour of the extinction points is probably related to the standards adopted in the industry (extinction considered as ended at the 95% of the transition) and consequently adopted in the code algorithm through an abrupt increase to 100%. This

statement is currently under verification with software developer.

In Fig. 12 for profile A and 13 for profile B, the numerical and experimental material replacements on the profile cross section are shown. Concerning simulation outputs, colours are related to the material extinction distance ‘d’ from stop mark (i.e. in Fig. 12 points in blue are replaced by new billet material in a profile section positioned at around 200 mm distance from stop mark, while red points required a greater transition of around 800 mm). In both profiles, the onset of the new billet material occurs in the centre of the profile, then enlarging up to filling all the sections.

In profile A, the experimental filling of the jagged detail occurs more slowly compared to the numerical prediction in which the filling takes place almost instantaneously: this is a consequence of the rapid increase of the numerical defect contamination from the 95% to the 100%. In fact, as shown in Fig. 12, the red area on the jagged detail is filled at the same distance from the stop mark while the experimental analysis shows a gradual filling. In profile B, the difference between the numerical and experimental outcomes is detected in the right part of the profile (as shown in Fig. 13) which, according to the simulation, is filled almost at the same distance from the stop mark, and, according to the experiments, more gradually.

The accuracy of the results using the QForm code is well aligned with the prediction obtained by other FEM codes found in the literature (Ref 16-18) or performed by the authors (Ref 13-15). Indeed, the charge weld prediction obtained by using different FEM codes approaches always provides a good matching with experimental data as further confirmation of the reliability of the FEM codes for analyses and optimization of the aluminium extrusion process.

## 5. Conclusions

In the present work, experimental and numerical investigations were carried out for evaluating the accuracy of the QForm Extrusion FEM code in the prediction of charge welds evolution on two solid extruded profiles made by AA6063 and AA6082 aluminium alloys. The quality of the estimations made by the theoretical formulas reported in the literature was also assessed. The main outcomes of this work can be summarized as follows:

- A very good numerical-experimental matching was found for the two investigated solid profiles in terms of charge weld onset and overall curve shape matching with a peak

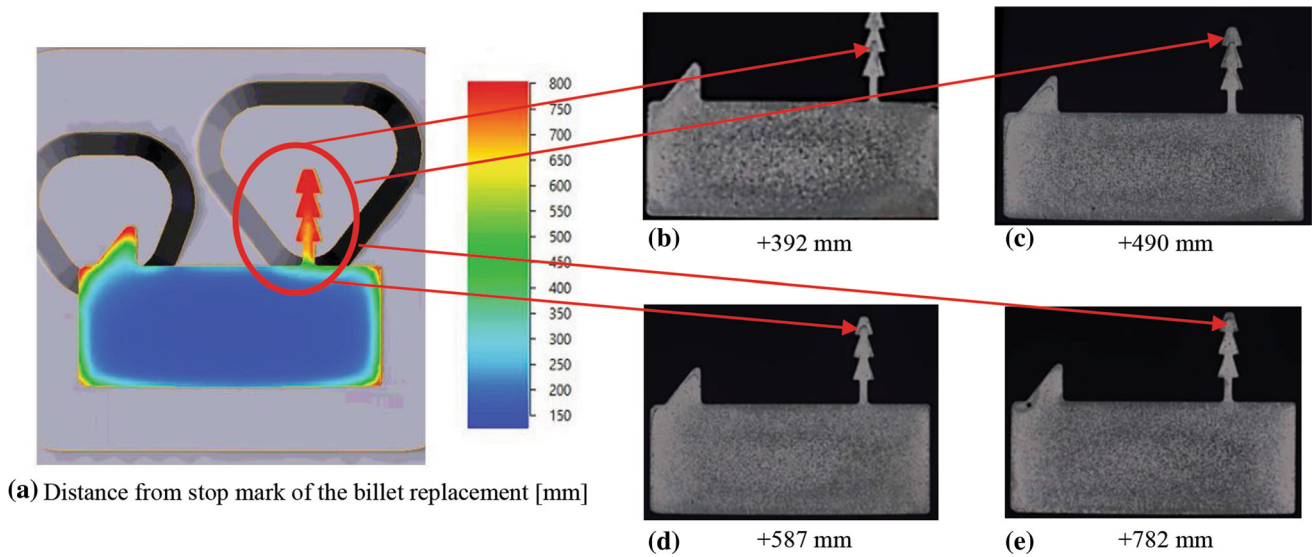


Fig. 12 Material replacement on profile A—(a) numerical, (b)–(e) experimental

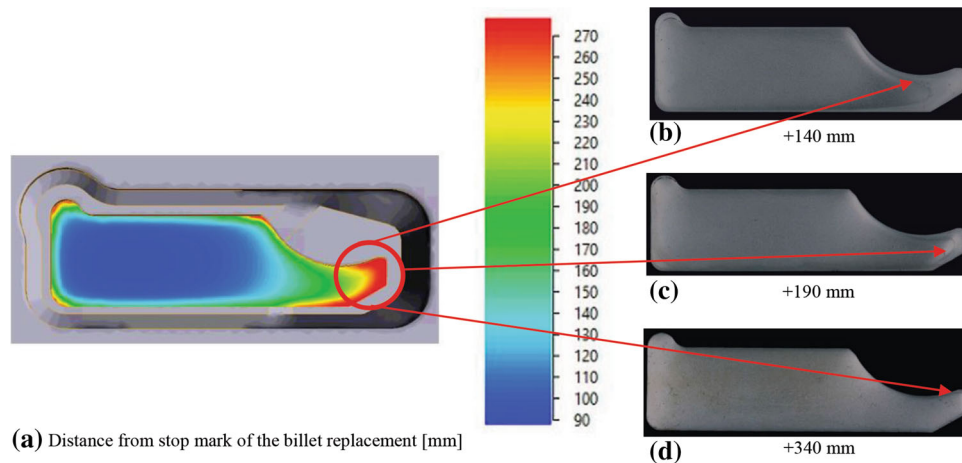


Fig. 13 Numerical and experimental material replacement on profile B—(a) numerical, (b)–(d) experimental

discrepancy of 122 mm.

- The main numerical-experimental difference was detected, for both profiles, in the last 5% of contamination. However, this can be neglected accounting for the industrial practice of considering the defect ended at the 95% of the old-new billet replacement.
- A good correlation between numerical predictions and experimental data was found also in terms of material replacement evolution on the cross section of the profiles.
- Theoretical formulas reported in the literature deeply underestimate the charge weld extent with a peak error of 72%.

## References

1. N. Hashimoto, Application of Aluminum Extrusions to Automotive Parts, *Kobelco Technol. Rev.*, 2017, **35**, p 69–75
2. N. Parson, J. Fourmann, J.F. Beland, Aluminum Extrusions for Automotive Crash Applications, SAE Technical Papers, 2017, March, p 1–16
3. J. Hirsch, Automotive Trends in Aluminium - The European Perspective, *Mater. Forum*, 2004, **28**(3), p 15–23
4. H. Valberg, Extrusion Welding in Aluminium Extrusion, *Int. J. Mater. Prod. Technol.*, 2002, **17**(7), p 497–556
5. A.J. Den Bakker, L. Katgerman and S. Van Der Zwaag, Analysis of the Structure and Resulting Mechanical Properties of Aluminium Extrusions Containing a Charge Weld Interface, *J. Mater. Process. Technol.*, 2016, **229**, p 9–21
6. A.A. Ershov, V.V. Kotov, YuN. Loginov. Capabilities of QForm-Extrusion Based on an Example of the Extrusion of Complex Shapes, *Metallurgist*, 2012, 55(9-10), p 695-701
7. M.B. Güner, C. Mehmetlioğlu, O.H. Çelik, M. Konar, G. Özçelik, Effect of Extrusion Parameters on Microstructural and Mechanical Properties of EN AW 6063, *Light Metals 2020*, A. Tomsett, Ed., Feb 23-27, 2020 (San Diego, CA, Springer: Cham, 2020), p 425-432
8. P. Chathuranga, Case Study of Extrusion Die Design Optimization Using Innovative Cartridge Type Die, *Light Metal Age*, 2014, **77**(5), p 20–27
9. X.R. Li, W.L. Fang, D. Tang, Y.L. Sun and D.Y. Li, Numerical Simulation on Hot Extrusion Forming of Aluminum Alloy Micro-Multiport Profile, *J. Plast. Eng.*, 2017, **24**(5), p 1–6

10. N. Biba, S. Stebunov and A. Lishny, Simulation of Material Flow Coupled with Die Analysis in Complex Shape Extrusion, *Key Eng. Mater.*, 2014, **585**, p 85–92
11. A.J. Den Bakker, L. Katgerman and S. Van Der Zwaag, Analysis of the Structure and Resulting Mechanical Properties of Aluminium Extrusions Containing a Charge Weld Interface, *J. Mater. Process. Technol.*, 2016, **229**, p 9–21
12. N. Nanninga, C. White and R. Dickson, Charge Weld Effects on High Cycle Fatigue Behavior of a Hollow Extruded AA6082 Profile, *J. Mater. Eng. Perform.*, 2011, **20**, p 1235–1241
13. M. Negozio, R. Pelaccia, L. Donati, B. Reggiani, L. Tomesani, T. Pinter, FEM Validation of front end and back end defects evolution in AA6063 and AA6082 aluminum alloys profiles, *Procedia Manufacturing*, Volume 47, M. Bambach, Ed., May 4-8, 2020 (Cottbus, DE), Elsevier Ltd., 2020, p 202-208
14. B. Reggiani and L. Donati, Experimental, Numerical, and Analytical Investigations on the Charge Weld Evolution in Extruded Profiles, *Int. J. Adv. Manuf. Technol.*, 2018, **99**(5–8), p 1379–1387
15. B. Reggiani, T. Pinter and L. Donati, Scrap Assessment in Direct Extrusion, *Int. J. Adv. Manuf. Technol.*, 2020, **107**(5–6), p 2635–2647
16. S. Lou, Y. Wang, C. Liu, S. Lu, S. Liu and C. Su, Analysis and Prediction of the Billet Butt and Transverse Weld in the Continuous Extrusion Process of a Hollow Aluminum Profile, *J. Mater. Eng. Perform.*, 2017, **26**(8), p 4121–4130
17. C. Zhang, Y. Dong, G. Zhao, L. Chen, Experimental and numerical investigations on transverse weld of hollow aluminum profile during porthole extrusion process, *Procedia Engineering*, Volume 207, J. Allwood, Ed., Sept 17-22, 2017 (Cambridge, UK), Elsevier Ltd., 2017, p 1653–1658
18. C. Zhang, Y. Dong, C. Wang, G. Zhao, L. Chen and W. Sun, Evolution of Transverse Weld During Porthole Extrusion of AA7N01 Hollow Profile, *J. Mater. Process. Technol.*, 2017, **248**(May), p 103–114
19. C. Zhang, G. Zhao, H. Chen, Y. Guan, H. Cai and B. Gao, Investigation on Effects of Die Orifice Layout on Three-Hole Porthole Extrusion of Aluminum Alloy 6063 Tubes, *J. Mater. Eng. Perform.*, 2013, **22**, p 1223–1232
20. T. Hatzebichler and B. Buchmayr, Finite Element Method Simulation of Internal Defects in Billet-to-Billet Extrusion, *Proc. Inst. Mech. Eng. Part B J. Eng. Manuf.*, 2010, **224**(7), p 1029–1042
21. Y. Mahmoodkhani, M.A. Wells, N. Parson and W.J. Poole, Numerical Modelling of the Material Flow During Extrusion of Aluminium Alloys and Transverse Weld Formation, *J. Mater. Process Technol.*, 2014, **214**, p 688–700
22. P. Saha, Quality issues of hollow extrusions for aerospace applications, Proceedings of the 9th aluminum extrusion technology seminar, Volume 1, May 13-16, 2008 (Orlando, FL), ET Foundation, 2008, p 441-458
23. C. Jowett, J. Adams, C. Daughetee, G. Lea, O.A. Huff, N. Fossil, Scrap Allocation, Proceedings of the 9th Aluminum Extrusion Technology Seminar, Volume 1, May 13-16, 2008 (Orlando, FL), ET Foundation, 2008, p 223-244
24. <https://qform3d.com>
25. J. Donea, A. Huerta, J.P. Ponthot, A. Rodriguez-Ferran, Arbitrary Lagrangian-Eulerian methods, *Encyclopedia of computational mechanics*, 2004, p 413-433
26. A. Hensel and T. Spittel, *Kraft Und Arbeitsbedarf Bildsamer Formgebungsverfahren*, 1, VEB Deutscher Verlag für Grundstoffindustrie, Auflage, Leipzig, 1978
27. M. El Mehtedi, S. Spigarelli, F. Gabrielli, L. Donati, Comparison study of constitutive models in predicting the hot deformation behavior of AA6060 and AA6063 aluminium alloys, *Materials Today: Proceedings*, Volume 2, Issue 10, Part A, L. Donati, L. Tomesani, Eds., May 12-16, 2015 (Firenze, IT), S. Bland, 2015, p 4732–4739
28. A. Selvaggio, T. Kloppenborg, M. Schwane, R. Hölker, A. Jäger, L. Donati, L. Tomesani, A.E. Tekkaya, Extrusion benchmark 2013 - Experimental analysis of mandrel deflection, local temperature and pressure in extrusion dies, *Key Engineering Materials*, Volume 585, A. E. Tekkaya, A. Jäger, Eds., May 14-18 (Milano, IT), Trans Tech Publications Ltd., 2013, p 13-22
29. J.Q. Yu, G.Q. Zhao and L. Chen, Investigation of Interface Evolution, Microstructure and Mechanical Properties of Solid-State Bonding Seams in Hot Extrusion Process of Aluminum Alloy Profiles, *J. Mater. Process. Technol.*, 2016, **230**, p 153–166
30. T. Hatzebichler, B. Buchmayr and A. Umgeher, A Numerical Sensitivity Study to Determine the Main Influence Parameters on the Back-End Defect, *J. Mater. Process. Technol.*, 2007, **182**, p 73–78
31. Y. Mahmoodkhani, M. Wells, N. Parson, C. Jowett and W. Poole, Modeling the Formation of Transverse Weld During Billet-on-Billet Extrusion, *Materials*, 2014, **7**(5), p 3470–3480

**Publisher's Note** Springer Nature remains neutral with regard to jurisdictional claims in published maps and institutional affiliations.